5 Studying the Details of the Electron–Electron Interaction in Solids and Surfaces

J. Kirschner, C. Winkler, and J. Berakdar

5.1 Introduction

Recently substantial experimental advances have been achieved in the energy-, spin- and angular-resolved detection of electron pairs that are simultaneously emitted from solid surfaces following excitation by electron or photon beams [1–14]. This process, which is for electron impact also called (e,2e) (one electron in, two electrons out) is visualized schematically in Figure 5.1. The (e,2e) studies from surfaces can be categorized in two broad classes: 1) *the transmission* and 2) *the reflection mode* experiments [1,2]. The transmission mode experiments are reviewed in Chapter 7. In this kind of experimental arrangement the incoming energetic electron traverses a free-standing thin film. The two emitted electrons are detected on the side of the film that does not contain the incident beam, i.e. both final-state electrons propagate in the forward direction with respect to the incoming beam. A typical reflection mode set-up is shown schematically in Figure 5.1. All the incoming and outgoing vacuum electrons are detected in the same half plane. The information obtainable from the (e,2e) measurements is quite different depending on the experimental arrangement and on the energies and momenta of the vacuum electrons, as discussed below.

5.2 General Considerations

To appreciate the significance of the (e,2e) process it is instructive to inspect the structure of the (e,2e) transition probability $W(\boldsymbol{k}_0, \boldsymbol{k}_1, \boldsymbol{k}_2)$

$$W(\boldsymbol{k}_0, \boldsymbol{k}_1, \boldsymbol{k}_2) \propto \sum_{\substack{i_{\rm occ} \\ \boldsymbol{k}}} |\langle \Psi_{\boldsymbol{k}_1,\boldsymbol{k}_2} | T_{\rm (e,2e)} | \varphi_{\boldsymbol{k}_0} \chi_{i_{\rm occ}\boldsymbol{k}} \rangle|^2 \delta(E_1 + E_2 - E_0 - \varepsilon_{\rm i}). \tag{5.1}$$

Here E_1, E_2 are the energies of the emitted electrons that are described by the final-state wavefunction $\Psi_{\boldsymbol{k}_1,\boldsymbol{k}_2}$ ($\boldsymbol{k}_1, \boldsymbol{k}_2$ are the electrons' wave vectors). The initial electronic states of the target are characterized by the single-particle orbitals $\chi_{i_{\rm occ}\boldsymbol{k}}$, where $\boldsymbol{k}$ is the Bloch wave vector and the index $i_{\rm occ}$ characterizes all other quantum numbers needed to specify the state of the surface. The incoming electron beam is described by the wavefunction $\varphi_{\boldsymbol{k}_0}$. The operator $T_{\rm (e,2e)}$ induces the transition from the initial state $|\varphi_{\boldsymbol{k}_0}\chi_{i_{\rm occ}\boldsymbol{k}}\rangle$ into the final state $\langle \Psi_{\boldsymbol{k}_1,\boldsymbol{k}_2}|$ while conserving the total energy.

Correlation Spectroscopy of Surfaces, Thin Films, and Nanostructures. Edited by Jamal Berakdar, Jürgen Kirschner

ISBN: 3-527-40477-5

Equation (5.1) can be re-written (exactly) as the expectation value of an effective operator M, where

$$W \propto \langle \Psi_{\boldsymbol{k}_1,\boldsymbol{k}_2} | M | \Psi_{\boldsymbol{k}_1,\boldsymbol{k}_2} \rangle, \tag{5.2}$$

$$M = \sum_{\substack{i_{\rm occ} \\ \boldsymbol{k}}} T_{\rm (e,2e)} |\varphi_{\boldsymbol{k}_0}\chi_{i_{\rm occ}\boldsymbol{k}}\rangle\langle\varphi_{\boldsymbol{k}_0}\chi_{i_{\rm occ}\boldsymbol{k}}| \delta(E_1 + E_2 - E_0 - \varepsilon_{\rm i}) T^{\dagger}_{\rm (e,2e)}. \tag{5.3}$$

To illustrate the kind of information that can be gained from an (e,2e) experiment we proceed as follows: If in Eq. (5.3) the transition operator $T_{\rm (e,2e)}$ does not depend on the properties of the occupied states[1] we operate within the prior form of scattering theory (i.e. we start from an asymptotic uncorrelated state $|\varphi_{\boldsymbol{k}_0}\chi_{i_{\rm occ}\boldsymbol{k}}\rangle = |\varphi_{\boldsymbol{k}_0}\rangle \otimes |\chi_{i_{\rm occ}\boldsymbol{k}}\rangle$) and then write M as

$$M = T_{\rm (e,2e)} |\varphi_{\boldsymbol{k}_0}\rangle \left\{ \sum_{\substack{i_{\rm occ} \\ \boldsymbol{k}}} |\chi_{i_{\rm occ}\boldsymbol{k}}\rangle\langle\chi_{i_{\rm occ}\boldsymbol{k}}| \delta(E_1 + E_2 - E_0 - \varepsilon_{\rm i}) \right\} \langle\varphi_{\boldsymbol{k}_0}| T^{\dagger}_{\rm (e,2e)}$$

$$= \int {\rm d}\boldsymbol{q}{\rm d}\boldsymbol{q}' \; T_{\rm (e,2e)} |\varphi_{\boldsymbol{k}_0}\boldsymbol{q}\rangle\langle\boldsymbol{q}'\varphi_{\boldsymbol{k}_0}| T^{\dagger}_{\rm (e,2e)}$$

$$\times \left\{ \sum_{\substack{i_{\rm occ} \\ \boldsymbol{k}}} \chi_{i_{\rm occ}\boldsymbol{k}}(\boldsymbol{q}) \chi^{*}_{i_{\rm occ}\boldsymbol{k}}(\boldsymbol{q}') \delta(E_1 + E_2 - E_0 - \varepsilon_{\rm i}) \right\},$$

$$M = -\frac{1}{\pi} \int {\rm d}\boldsymbol{q}{\rm d}\boldsymbol{q}' \; T_{\rm (e,2e)} |\varphi_{\boldsymbol{k}_0}\boldsymbol{q}\rangle \; {\rm Im}\, G(\boldsymbol{q}, \boldsymbol{q}', E) \; \langle\boldsymbol{q}'\varphi_{\boldsymbol{k}_0}| T^{\dagger}_{\rm (e,2e)}. \tag{5.4}$$

In the second line of this equation we inserted a complete set of plane wave ($\int {\rm d}\boldsymbol{q}|\boldsymbol{q}\rangle\langle\boldsymbol{q}|$). The expression in the wavy brackets is the non-local spectral density which is expressible in terms of the imaginary part of the retarded Green's function of the surface $G(\boldsymbol{q}, \boldsymbol{q}', E)$. The latter is evaluated at the energy $E = (E_1 + E_2) - E_0$ that is determined experimentally (all energies are measured with respect to the vacuum level). Inserting Eq. (5.4) into Eq. (5.2) one deduces that

$$W \propto -\int {\rm d}\boldsymbol{q}{\rm d}\boldsymbol{q}' \; \langle \Psi_{\boldsymbol{k}_1,\boldsymbol{k}_2}| \, T_{\rm (e,2e)} \, |\varphi_{\boldsymbol{k}_0}\boldsymbol{q}\rangle\langle\varphi_{\boldsymbol{k}_0}\boldsymbol{q}'| \, T_{\rm (e,2e)} \, |\Psi_{\boldsymbol{k}_1,\boldsymbol{k}_2}\rangle \; {\rm Im}\, G(\boldsymbol{q}, \boldsymbol{q}', E) \tag{5.5}$$

5.3 Results and Interpretations

The usefulness of the exact mathematical exercise presented above becomes now apparent: Equation (5.5) contains three important physical quantities: 1. The hole non-local spectral density ${\rm Im}\, G(\boldsymbol{q}, \boldsymbol{q}', E)$. 2. The electron–electron interaction $T_{\rm (e,2e)}$ and 3. the correlated electron-pair wavefunction $\Psi_{\boldsymbol{k}_1,\boldsymbol{k}_2}$. Choosing the appropriate experimental set-up one can focus on each of these quantities separately. E.g., if we assume that $T_{\rm (e,2e)}$ depend only on

[1] This is not always the case, e.g. for certain elements $T_{\rm (e,2e)}$ is spin dependent (for example due to spin–orbit coupling) and hence it depends on the spin-quantum numbers of the electronic states of the surface.

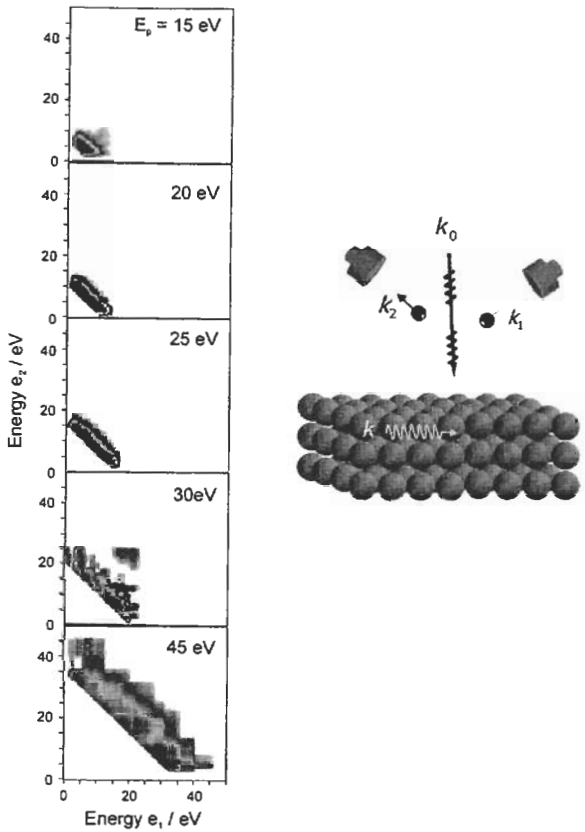

Figure 5.1: A schematic representation of the (e,2c) experimental set-up in the reflection mode geometry is shown on the right hand side. The left part shows a series of energy-distribution spectra of the electron pairs at various impact primary energies shown on the figures ($E_0 = 15$ eV, 20 eV, 25 eV, 30 eV) and $E_0 = 45$ eV. The incoming electron wave vector is perpendicular to the surface (a Cu(001) surface) and the two electrons are emitted symmetrically to the left and to the right of the surface normal at an angle of 40°. The absolute values of the (e,2e) emission probability are not determined experimentally. See also color figure on page 229.

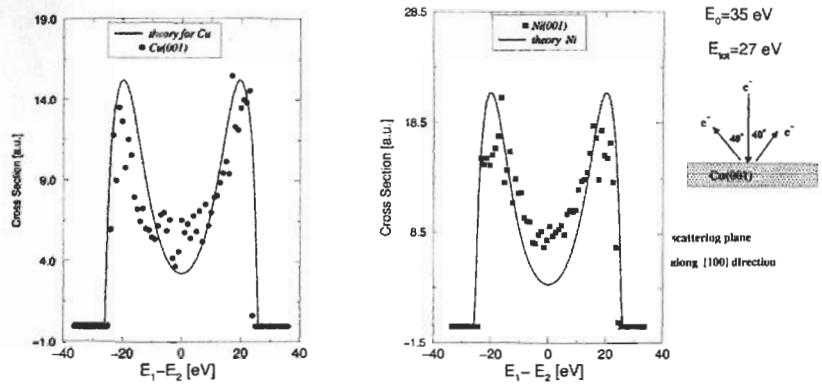

Figure 5.2: The excess energy-sharing of the escaping electron pair with a fixed total pair energy $E_{\rm tot} = 27$ eV. The incident energy is fixed to $E_0 = 35$ eV. Experimental and theoretical results are shown for a Cu(001) crystal (left panel) and a Ni(001) crystal (right panel). As schematically shown in the figure, the incoming beam is normal to the surface, whereas the two emitted electrons are detected at 40° to the left and to the right of the surface normal. The experiments are determined on a relative scale only.

the inter-electron distance and that the vacuum electrons in the initial and the final states occupy plane waves, one finds that $\boldsymbol{q} = \boldsymbol{q}' = \boldsymbol{k}_1 + \boldsymbol{k}_2 - \boldsymbol{k}_0$. Under these assumptions, which are justified at high energies and in the transmission mode, one can study the single-particle Bloch spectral function $\mathrm{Im}\, G(\boldsymbol{q}, \boldsymbol{q}, E)$, as evident from Eq. (5.5). Such studies are reviewed in Chapter 7. On the other hand, as explained in full detail in Chapter 2, the electron–electron interaction in a many-body system has a rich structure due to the cooperative, correlated behavior of the electrons that results in screening, non-locality and a frequency dependence of $T_{(\mathrm{e,2e})}$. Some experiments to study the properties of $T_{(\mathrm{e,2e})}$ by means of (e,2e) have already been performed [15] (e.g. by tuning the incoming beam wave vector to the plasmon modes of the surface).

The information on the details of interaction between the excited electrons as described by $\Psi_{\boldsymbol{k}_1,\boldsymbol{k}_2}$ can also be singled out, to a large extent, by virtue of the following observation: The energy- and wave-vector conservation laws dictates that $E = E_1 + E_2 - E_0$, $\boldsymbol{q}_\parallel = \boldsymbol{k}_{1\parallel} + \boldsymbol{k}_{2\parallel} - \boldsymbol{k}_{0\parallel} - \boldsymbol{G}\boldsymbol{G}_\parallel = \boldsymbol{q}'$. These laws are also expressible in the form

$$\epsilon_{\rm i} = E_1 + E_2 - E_0, \tag{5.6}$$

$$\boldsymbol{k}_{1\parallel} + \boldsymbol{k}_{2\parallel} = \boldsymbol{k}_{0\parallel} + \boldsymbol{k} + \boldsymbol{G}\boldsymbol{G}_\parallel. \tag{5.7}$$

Here $\boldsymbol{G}\boldsymbol{G}_\parallel$ is a surface reciprocal lattice vector. Therefore, we can tune the parameters of the experimental set-up to a certain initially occupied electronic state. E.g., for the (e,2e) coincidence spectra shown in Figure 5.1, all coincidence signals appearing at a constant total energy of the pair $E_{\rm tot} = E_1 + E_2 = \text{const.}$ originate from the same energy state in the sample (throughout this paper we neglect the effect of inelastic multiple scattering). As deduced from Eq. (5.6), fixing E_0 and varying $E_{\rm tot}$ means varying the initial binding energy $\epsilon_{\rm i}$. This kind of

scan can be equally achieved if E_{tot} is fixed and E_0 is varied. Both alternatives are realized in Figure 5.1. To zoom in on the detailed structures present in the density plot shown by Figure 5.1 we choose a certain but fixed E_{tot} = const. I.e. we fix in energy space the initially occupied state of the surface. Then we can vary E_1 and E_2 (while keeping $E_1 + E_2$ = const.) and study the energy correlation within the pair. This kind of study is performed in Figure 5.2 for Cu(001) and Ni(001). Details of the calculations as well as the technical details of the experiments can be found in various publications (e.g. Refs. [2–7, 9, 11, 12] and references therein). The point which we would like to discuss here in some detail is the typical symmetric shape of the measured spectra with respect to the equal energy point $E_1 = E_2$. This symmetry seems plausible from a geometrical point of view. In reality it is a profound manifestation of the exchange interaction and hence is a signature of one type of electronic correlation. To appreciate this fact we consider in Figure 5.3 a nonsymmetric situation. Figure 5.3(a) shows the calculations neglecting the exchange effects, i.e. when we assume the two electrons to be distinguishable.

Furthermore we consider two situations: Detecting the projectile electron to the right of the incoming beam (at 30°) we obtain the theoretical results shown by the dashed curve. In contrast, if the projectile electron is detected left of the incident beam the dotted curve is obtained. As clear from Figure 5.3(a) the origin of the peaks in the full calculations (including exchange) are certain peaks in the direct and in the exchange scattering probabilities. On the other hand the peaks occurring in the dashed and dotted curves in Figure 5.3(a) are due to the following fact. At moderate and high energies, the quantum electron–electron scattering is most probable when the momentum transfer from one (projectile) electron to the other electron is small. Hence, after being elastically reflected back from the crystal the projectile electron transfers, via electron–electron scattering, little energy to a bound electron and escapes thus with an energy similar to its initial one. In a solid however the bound electron also has a well-defined crystal momentum that varies depending on the initial state. This initial crystal momentum distribution may even dominate the outcome of the encounter with the projectile, as illustrated in Figure 5.3(b–d) where for a fixed impact energy E_0 the kinetic energy E_{tot} is lowered, meaning that the bound electron resides in deeper levels in the conduction band. For all cases Figure 5.3(a–d), it is clear that in the symmetric situation, where both electrons are detected at equal angles (30°) with respect to the incoming beam, the cross section will be symmetric with respect to the equal energy point. In this sense, the symmetric geometry is less favorable for the study of the scattering dynamics.

It should be noted however that the double peak structure of the energy-sharing in Figure 5.2 will change at very low energies to a single flat peak at equal energies. The reason for this is that, quantum mechanical low energy scattering is dominated by s-wave (i.e. isotropic) scattering. On the other hand the electron-pair emission probability has to vanish at $E_1 \to 0$ or $E_2 \to 0$ which in combination with the isotropy of low energy scattering results in one single flat peak at $E_1 = E_2$.

A single peak structure in the energy-sharing distribution can also be obtained at higher energies, but at different emission angles of the electrons, as demonstrated in Figure 5.4 for the case of symmetric electron emission angles with respect to the surface normal. For the emission angles $\theta_1 = \theta_2 = 35°$ we observe the double peak structure, the origin of which has been discussed above. However, when the emission angles are increased the energy region where pair emission may occur shrinks. At $\theta_1 = \theta_2 = 70°$ one single peak at $E_1 = E_2$

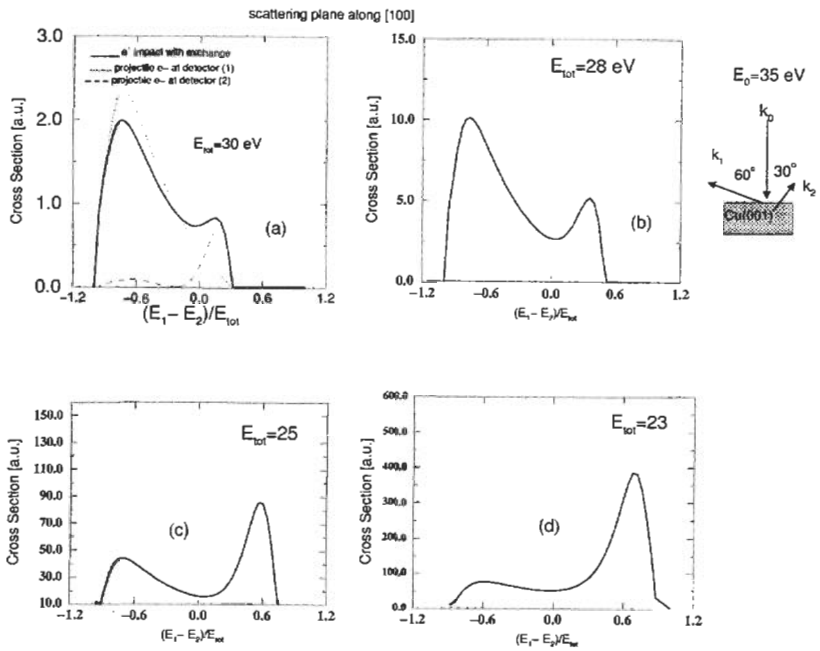

Figure 5.3: The same impact energy as in Figure 5.2 but with varying E_{tot}. In addition one of the detectors (labelled 2) is fixed at an angle of 30° to the right of the surface normal whereas the other detector (detector 1) is located at 60° to the left of the incoming beam (cf. schematic drawing). The solid curves in (a–d) are the theoretical (e,2e) probability calculated taking account of the exchange effects. In (a) the calculations shown by the dotted and dashed lines are performed while neglecting exchange within the electron pair. The dotted (dashed) line is the outcome of the calculations when the projectile electron is detected with the detector 1 (2). The sample is a Cu(001) single crystal and all vectors (k_0, k_1, k_2) are in one plane (the scattering plane).

is observed, which is actually rather due to the absence of the two peaks at the low energy wings for the case $\theta_1 = \theta_2 = 35°$. The shrinking in Figure 5.4(a),(b) of the energy window for the electron pair emission is dictated by the conservation law for the parallel components of the wave vectors. With increasing emission angles the parallel wave vector component of the fast electron (at the low energy wings) increases. The wave vector conservation law requires however, that the initial state (from which the electron is knocked out) has to contain an equally large parallel-wave vector component. If this is not the case the pair emission is prohibited.

The above discussions and interpretations of the electron-pair spectra did not involve directly the influence of the crystal. However, it is clear that effects such as those shown in

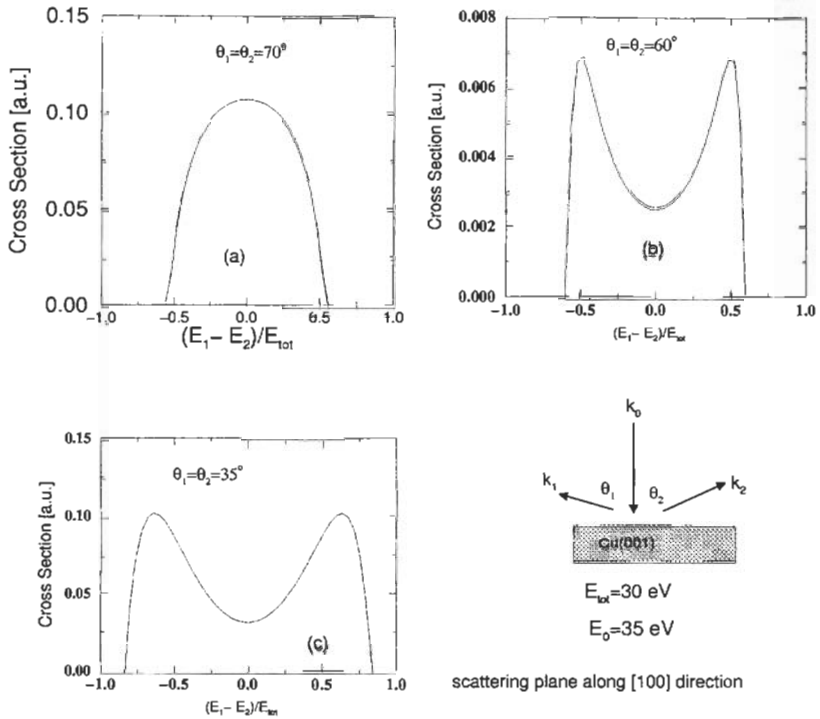

Figure 5.4: The same as in Figure 5.2 however the emission angles of the two electrons are varied as shown on the individual panels. The target is a Cu(001) single crystal.

Figure 5.3 cannot occur in an atomic or a molecular target (for an atomic or a molecular system usually one single discrete bound state is involved in the process and the wave vector is not a good quantum number). In addition, from phase-space consideration one can show [11] that the electron-pair emission probability scales as $k_1 k_2$. Therefore, all the spectra shown above vanish when $E_1 \rightarrow 0$ or $E_2 \rightarrow 0$. This is not the case for an atomic or a molecular target. The reason for this is that, in contrast to metal surfaces, the single electron density of states in an atomic target diverges at threshold as $1/k_{1,2}$. Incidentally this divergence is canceled out by the phase-space factor $k_1 k_2$ and the (e,2e) energy-sharing spectra for atomic or molecular targets are finite when $k_{1,2} \rightarrow 0$.

The ordering of the crystal potential also has a profound influence on the electron-pair energy spectra. A spectrum of a single electron scattered from an ordered multi-center potential shows well-known diffraction patterns [16, 17]. In analogy, two electrons can also be

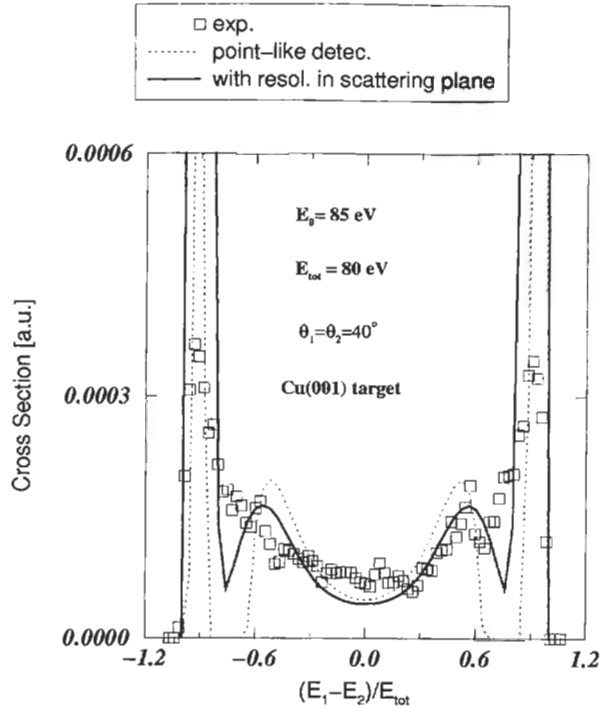

Figure 5.5: The same as in Figure 5.2, however the incident energy is increased to E_i = 85 eV and the pair total energy is fixed at $E_{\text{tot}} = 80$ eV. The calculations are shown with (solid curve) and without (dotted curve) account for the finite experimental angular resolution (same resolution as in Ref. [3]). Experiments and calculations are performed for a Cu(001) single crystal. The experiments are determined on a relative scale only.

diffracted from the crystal potential, resulting in electron-pair diffraction [3]. As observed in Figure 5.5, when the initial total wave vector of the electron pair $\boldsymbol{k}_{o\parallel} + \boldsymbol{k}_{\parallel}$ is changed by a multiple of a reciprocal lattice vector, diffraction peaks appear. In the experiment these peaks are less pronounced due to the finite experimental resolution (more examples of the pair diffractions are found in Refs. [3, 18]). In this context it should be remarked that the interaction of the electrons with the crystal potential is usually assumed to be of a single particle nature (but the potential has a multi-center character). Thus, in single-particle terms one can say that one of the electrons is diffracted from the crystal potential and subsequently collides with the other electron. Since the two electrons can exchange momentum, the single particle diffraction peaks are then diffused. On the other hand, other peaks appear due to the conser-

vation of the electron-pair parallel wave vector moduli a reciprocal lattice vector, as expressed by Eq. (5.7). This argument does not rely on which scattering process occurs first. The key point here is that the electron-pair diffraction depends crucially on the momentum transfer within the electron pair and hence it is a direct manifestation of the interaction between the two electrons. This is quite the opposite situation to the diffraction process of a single particle from a crystal potential which is hardly dependent on the electronic correlation.

5.4 Conclusions

The aim of this chapter is to present a small fraction of the rich phenomena that occur when an electron pair is excited from a surface. Here we have chosen to focus on the interpretation of the spin-averaged scattering from clean surfaces. The (e,2e) experiments and theories have evolved however to include the study of ferromagnets, semiconductors, wide-band gap insulators, alloys, clusters and adsorbates. The results of some of these studies are presented in Ref. [19] where further references can be found.

References

[1] S. Iacobucci, L. Marassi, R. Camilloni, S. Nannarone, and G. Stefani, Phys. Rev. B **51** (1995) 10252.

[2] O. M. Artamonov, S. N. Samarin, and J. Kirschner, Appl. Phys. A **65** (1997) 535.

[3] J. Berakdar, S. N. Samarin, R. Herrmann, and J. Kirschner, Phys. Rev. Lett. **81** (1998) 3535.

[4] J. Kirschner, O. M. Artamonov and A. N. Terekhov, Phys. Rev. Lett. **69** (1992) 1711.

[5] J. Kirschner, O. M. Artamonov and S. N. Samarin, Phys. Rev. Lett. **75** (1995) 2424.

[6] O. M. Artamonov, S. N. Samarin and J. Kirschner, Appl. Phys. A **65** (1997) 535.

[7] A. Morozov, J. Berakdar, S. N. Samarin, F. U. Hillebrecht, and J. Kirschner, Phys. Rev. B **65** (2002) 104425.

[8] S. A. Canney, M. Vos, A. S. Kheifets, X. Guo, I. E. McCarthy, and E. Weigold, Surf. Sci. **382**(1-3) (1997) 241.

[9] R. Feder, H. Gollisch, D. Meinert, T. Scheunemann, O. M. Artamonov, S. N. Samarin, and J. Kirschner, Phys. Rev. B **58** (1998) 16418.

[10] A. S. Kheifets, S. Iacobucci, A. Ruocco, R. Camiloni, and G. Stefani, Phys. Rev. B **57** (1998) 7360.

[11] J. Berakdar, M. P. Das, Phys. Rev. A **56** (1997) 1403.

[12] J. Kirschner, O. M. Artamonov, and S. N. Samarin, Phys. Rev. Lett. **75** (1995) 2424; O. M. Artamonov and S. N. Samarin, Tech. Phys. **46** (2001) 1179.

[13] K. A. Kouzakov, J. Berakdar, Phys. Rev. B **66** (2002) 235114.

[14] Z. Fang, R. S. Matthews, S. Utteridge, M. Vos, S. A. Canney, X. Guo, I. E. McCarthy, and E. Weigold, Phys. Rev. B **57** (1998) 12882.

[15] S. Samarin, J. Berakdar, A.Suvorova, O. M. Artamonov, D. K. Waterhouse, J. Kirschner, J.F. Williams, Surf. Sci. **548** (2004) 187-199.

[16] J. B. Pendry, *Low Energy Electron Diffraction* (Academic Press, London, 1974).

[17] M. A. van Hove, W. H. Weinberg, and C.-M. Chan, *Low Energy Electron Diffraction*, in Springer Series in Surface Science (Springer, Berlin 1986).

[18] S. Samarin, J. Berakdar, O. Artamonov, H. Schwabe, and J. Kirschner, Surf. Sci. **470** (2000) 141.

[19] *Many Particle Spectroscopy of Atoms, Molecules, Clusters, and Surfaces*, edited by J. Berakdar and J. Kirschner (Kluwer Academic/Plenum, New York, 2001).